DOI: 10.13009/EUCASS2017-535

Effects of Cu-alloy Material Properties on Lifetime of a Combustion Chamber with or without a Thermal Barrier Coating

Toshiya Kimura, Shin-ich Moriya*, and Masaharu Takahashi***
**Japan Aerospace Exploration Agency*
Kimigaya, Kakuda, Miyagi, 981-1525, Japan
*** Hitachi Solutions East Japan, Ltd.*
Honcho, Aoba, Sendai, Miyagi, 980-0014, Japan

Abstract
Possible factors to extend lifetime of a combustion chamber of a large thrust rocket engine were investigated. Tow-dimensional FEM simulations were conducted to estimate creep fatigue damage to the inner liner of a combustion chamber modelled for a large thrust rocket engine. For the combustion chamber with an inner liner of three different copper alloys, the effects of a thermal barrier coating and the material property of the outer shell on lifetime were examined. It was found that an appropriate combination of materials of the inner liner and the outer shell with a thermal barrier coating would extend the lifetime of a large thrust combustion chamber.

Nomenclature

A	=	area thermal diffusion time
c	=	specific heat
d	=	thickness
df	=	damage due to low cycle fatigue (LCF)
dc	=	damage due to creep
D	=	total damage
N_f	=	number of lifetime cycles of combustion chamber
N_r	=	number of cycles to rupture
T	=	average temperature during steady-state combustion
t_c	=	duration time of steady-state combustion
t_r	=	time to rupture due to creep
α	=	thermal diffusivity
$\Delta\varepsilon$	=	total strain range
k	=	thermal conductivity
λ	=	coefficient of thermal expansion
ρ	=	density
σ	=	average equivalent stress during steady-state combustion
τ	=	thermal diffusion time
subscript		
TBC	=	thermal barrier coating
Sb	=	substrate

1. Introduction

In the development of a reusable rocket engine, the combustion chamber is one of the most critical components which defines the lifetime of the engine. Very high pressure and temperature combustion gas flows inside the chamber, and

DOI: 10.13009/EUCASS2017-535

a very low temperature and high pressure coolant flows inside cooling channels. Combustion gas and coolant are separated by a wall made of a copper alloy with a thickness of only around 1mm. These conditions are drastically changed during the combustion cycle such as start-up, shutdown, and throttling operations. Hence, the inner liner of the combustion chamber suffers large and unsteady thermal stress change.

To extend the lifetime of a rocket engine combustion chamber, various concepts have been proposed [1, 2], and various approaches for prediction of lifetime have been made experimentally and analytically. Sun et al. [3, 4] conducted experiments to produce failure due to creep fatigue damages using a subscale combustion chamber and conducted finite element analysis to predict the failure. Riccius et al. [5-7] have attempted to revise the analysis method, experimental results being validated by used a flat panel heated by a laser (called TMF panel). A multi-physics coupled simulation, in which thermo-fluid coupled dynamics were solved between coolant flow and the chamber wall, was developed and applied to a rocket combustion chamber [8, 9]

At the Kakuda space center of JAXA, a reusable rocket engine was developed and hot firing tests were conducted from 2014 to 2015 [10, 11]. This engine was designed to be reused for 100 flights of a reusable sounding rocket [12]. Since the thrust of this engine was 40 kN with a relatively low chamber pressure of about 3.5 MPa, the combustion chamber could be designed by appropriately adjusting the operating conditions. Hot firing tests proved that the combustion chamber was reusable for over 100 flights.

However, for engines with a larger thrust of over 1000 kN, the chamber pressure should be much higher than that of the engine of the reusable sounding rocket. It will be very difficult to achieve such a high-pressure combustion chamber which is reusable over several tens or more flights by just adjusting the operating conditions. The present work, therefore, examined key factors to realize a long-life combustion chamber with a thrust of over 1000 kN, especially focusing on Cu-alloy materials of an inner liner, material properties of an outer shell, and a thermal barrier coating (TBC) on the inner surface of the chamber.

Two-dimensional finite element method (FEM) simulations were performed to estimate creep fatigue damages to the inner liner of the combustion chamber for the cross section at the throat region for different Cu-alloy materials of the inner liner and materials of the outer shell with or without TBC.

Simulation results showed that the lifetime of the inner liner of a combustion chamber was strongly affected by not only characteristics of a Cu-alloy of an inner liner but also by the material property of the outer shell such as the coefficient of thermal expansion. It was also found that the effect of the TBC depended on the material characteristics of the Cu-alloy of the inner liner. This work will provide key information useful for the development of long-life combustion chambers of high power reusable rocket engines.

2. Numerical analysis

2.1 Combustion chamber model

Figure 1 shows a typical structure of a combustion chamber and the cross section of the chamber wall. One of the major objectives of the present work was to examine the possibility of extending the lifetime of the combustion chamber of a large thrust rocket engine by using FEM analysis. To conduct simulations, it was necessary to create the shapes of the chamber wall and coolant channels of the combustion chamber with a thrust of over 1000 KN.

The LE-X rocket engine with a thrust of over 1400 kN was studied intensively as the next generation of the Japanese rocket engine [13,14]. Hence, as the model of the combustion chamber in the present study, especially the structure of the inner shape of the chamber and that of the coolant channels were created by modelling the combustion chamber of the LE-X rocket engine.

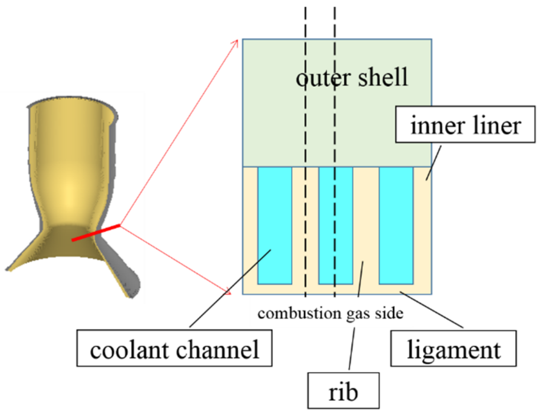

Figure 1: Schematic of the combustion chamber and a cross-section of the chamber wall

DOI: 10.13009/EUCASS2017-535

2.2 FEM model

For the estimation of damages due to low cycle fatigue and creep, the cross section of the chamber wall at the throat where the heat flux shows its maximum was modelled. The shapes of the coolant channel and the inner liner of the LE-X combustion chamber were used for the present model. Although the combustion chamber of the LE-X has a thick throat support [13], the outer shell of the present model was modelled by simplification to have the same thickness as that of the inner liner. With this thickness of the outer shell, the chamber wall was estimated to be able to withstand hoop stress due to the chamber pressure.

Since the coolant channels are located at regular intervals in the circumferential direction and each coolant channel has the same geometry, finite element mesh was created for one coolant channel with a half pitch, which is shown by an area between the two dashed lines in Fig.1.

The layer of the TBC was assumed to have thicknesses of 50 μm and 100 μm in the present model. In Fig. 2, FEM meshes without a TBC and with a TBC layer of 100 μm are shown. The spacing between nodes of the mesh is typically 15 μm. For this mesh size, the total number of nodes and elements are around 62 000 and 20 000, respectively.

The dependency of the present calculations on the mesh resolution was checked for several mesh resolutions, the spacing being changed from 8 μm to 60 μm. The mesh resolution with the spacing of 15 μm was the most appropriate one in view of both accuracy of solutions and computational cost.

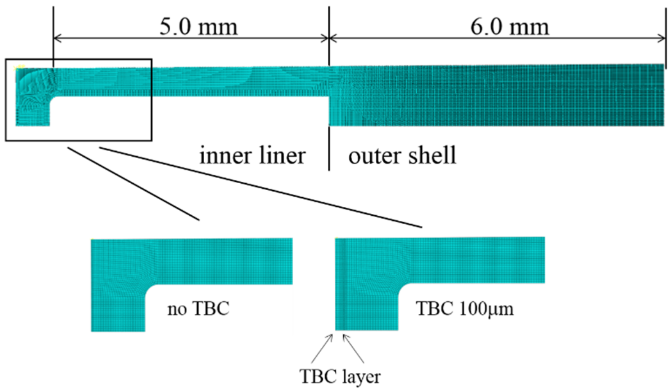

Figure 2: Finite element mesh of 2D cross-section of the combustion chamber wall

For the surface on the combustion gas side of the FEM model shown in Fig.2, the condition of the combustion gas at the throat was applied as a boundary condition. The temperature and pressure of the combustion gas were derived using a one-dimensional equilibrium code known as ODE [15]. The heat transfer coefficient at the throat was estimated from the Bartz equation [16].

For the surface of the coolant channel, the temperature, pressure, and heat transfer coefficient at the throat were applied as the boundary conditions. These values were derived by solving flow equations along the coolant channel from the inlet to the outlet using a quasi-one-dimensional coolant flow solver which was developed at JAXA.

2.3 Chamber wall materials

For the inner liner of a combustion chamber, a copper alloy is usually used due to its high thermal conductivity. Various copper alloys have been used for combustion chambers of rocket engines. For combustion chambers of rocket engines in Europe and United States, a copper alloy with zirconium and silver, which is called NARloy-Z [17], are mainly used. NASA has developed a copper alloy containing chromium and niobium, called GRCop [18], for reusable rocket engines.

For Japanese rocket engines, copper alloys with chromium and zirconium, CuCrZr, have been mainly used. In the present work, three different copper alloys with chromium and zirconium, named Cu-A, Cu-B, and Cu-C, were examined. In the manufacturing process, Cu-B is subjected to solution treatment and aging after hot forging. In processing Cu-A, a cold forging process is added between solution treatment and aging to improve mechanical properties. Cu-C is subjected to heat treatment during the brazing thermal cycle. Hence, Cu-A, B, and C are copper alloys with chromium and zirconium but have different characteristics, especially mechanical properties, due to different manufacturing processes.

DOI: 10.13009/EUCASS2017-535

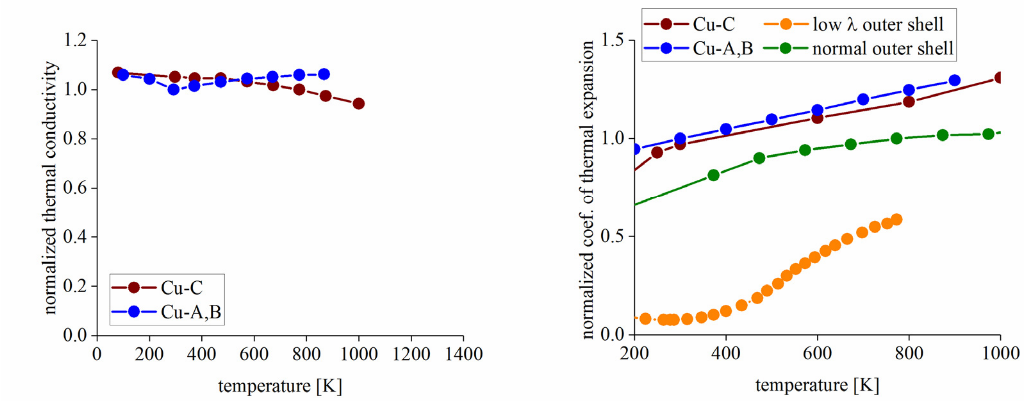

Figure 3: Normalized thermal conductivity (left) and coefficient of thermal expansion (right) for Cu-A, B, C, and materials for the outer shell

Figure 3 shows the physical properties, thermal conductivity and coefficient of thermal expansion, for materials used in the inner liner and outer shell. Cu-A and B have almost the same thermal conductivity and coefficient of thermal expansion. In the left of Fig. 3, thermal conductivities are plotted normalized by that of Cu-A (B) at room temperature. Coefficients of thermal expansion are also normalized by that of Cu-A (B) at room temperature and plotted in the right of Fig. 3. As shown in Fig. 3, thermal conductivity and the coefficient of thermal expansion of Cu-C are almost the same as those of Cu-A (B).

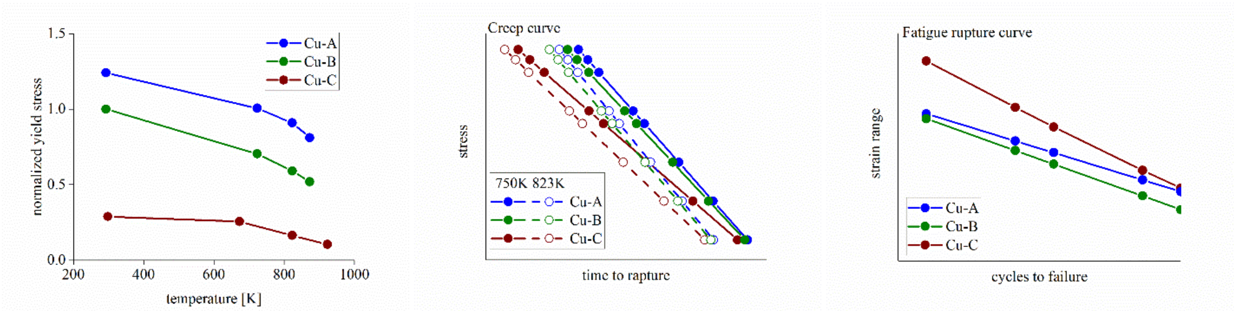

Figure 4: Normalized yield stress (left), creep curve (middle), and fatigue rupture curve (right) of Cu-A, B, and C

Figure 4 shows the mechanical characteristics for these alloys. Yield stresses are normalized by that of Cu-B at room temperature and plotted in the figure on the left. Creep and fatigue strengths are shown in the middle and right figures, respectively. The mechanical characteristics of these copper alloys show large differences. Especially the yield strength presents typical characteristic differences among these copper alloys. Cu-C is an alloy heat-treated during the brazing thermal cycle and its yield strength becomes much smaller than those of Cu-A and Cu-B. The creep and fatigue strengths of these alloys also show differences. The creep strength of Cu-A is highest and that of Cu-C is much lower than the others. The fatigue strength of Cu-C, on the other hand, is the highest among them. These differences of mechanical characteristics result in extension of lifetime as an inner liner material.

In the present paper, hereafter, the chamber wall model, in which the material of the inner liner is made of Cu-A, is called model A. The other models using the copper alloys Cu-B and Cu-C are called model B and model C, respectively.

In the present work, two types of the outer shell were assumed. One was a normal outer shell which was made of a high strength stainless steel. The other was a low λ outer shell which was characterized by low expansion.

As a material of the normal outer shell, a high strength stainless steel such as A286, was assumed. To examine the effect of restriction suffered by the outer shell during a combustion cycle on the inner liner, Invar, an alloy with a very low coefficient of thermal expansion, was used for the low λ outer shell in the present simulation. The normalized coefficients of thermal expansion of these materials are presented in Fig. 3.

Although the applicability of Invar to the outer shell of a rocket engine combustion chamber should be investigated, the main objective in this study was to examine the effect of restriction by the outer shell on lifetime of the inner liner. Hence, discussion of the applicability of Invar is not pursued in this paper.

2.4 Inelastic model

The chamber wall of a reusable rocket engine will be subjected to cyclic thermal stress loading in an inelastic region. In the present work, ABAQUS/standard (ver.6.14) was used. To simulate behaviour of materials of a chamber wall, a nonlinear isotropic/kinematic combined hardening model in ABAQUS were used. For these copper alloys, uniaxial tensile fatigue tests were conducted at several temperatures. The parameters to define the nonlinear kinematic hardening law in ABAQUS were defined from the 1st cycle data of fatigue tests, and those of the isotropic hardening properties were defined from several data sets between the 10th and 50th cycles. By using a nonlinear isotropic/kinematic hardening model of ABAQUS, the components of which were defined by experimental data of fatigue tests, each test was simulated with a 2D axisymmetric FEM model with the same conditions as those of the experiments. Figure 5 shows a comparison between calculated data and test data by a stress-strain hysteresis curve for the material of Cu-B at 873 K. The figures of the left and right show the 1st and 30th cycles, respectively. The open circles show the experimental results and the solid lines indicate the simulation results.

The discrepancies between calculations and experiments depend on the model. For some models, there are still large deviations. The main objective of the present work was not so much to predict the lifetime of a combustion chamber quantitatively as to investigate possible keys to extend the lifetime of a combustion chamber with a large thrust. Hence, an inelastic model was not further pursued in this work.

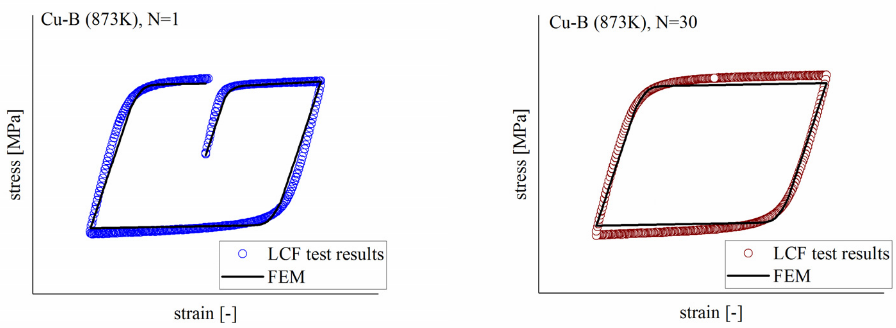

Figure 5: Comparison of fatigue test and FEM simulation for one of the uniaxial tensile fatigue tests of Cu-B. Stress-strain curves at 873 K for the 1st cycle (left) and the 30th cycle (right)

2.5 Estimation of low cycle fatigue and creep damages

In the present simulations, a typical combustion cycle was assumed to be start-up for 5 seconds, a steady state combustion phase for 400 seconds, shut-down for 2 seconds, and a chill-down phase for 2000 seconds. This combustion cycle was repeated three times. In the final cycle, the total range of equivalent strain, $\Delta\varepsilon$, average equivalent strain, σ, and average temperature, T, during a steady state combustion phase were estimated.

The number of cycles to rupture, N_r, was derived using $\Delta\varepsilon$ from the fatigue curve of each copper alloy. The time to rupture due to creep, t_r, was derived from the creep curve by using σ and T. The damages due to low cycle fatigue and creep were derived using the equation (1). The total damage was the summation of df and dc, assuming a linear cumulative damage rule.

Since equivalent stress showed a slight change with time even in the steady state combustion phase, the total creep damage was derived by integrating creep damages estimated in a short time inverval.

$$df = \frac{1}{N_r(\Delta\varepsilon)},\ dc = \frac{t_c}{t_r(\sigma,T)}, D = df + dc,\ N_f = \frac{1}{D} \quad (1)$$

DOI: 10.13009/EUCASS2017-535

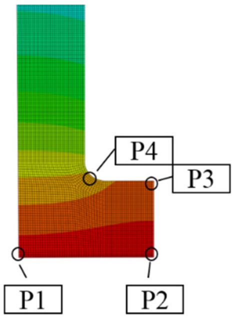

Figure 6: Damage evaluation points

Figure 6 shows positions to evaluate damages and lifetimes of the chamber wall. P1 is located at the center of a rib facing combustion gas. P2 and P3 are located at the center of a ligament facing combustion gas and coolant, respectively. P4 is located at the corner of the coolant channel. For these points of all models, damages were estimated, the total damage of P1 being the largest among all the present models. Hence, in this paper, effects on lifetime among models are discussed at the position P1.

For all models, calculations were conducted for three cycles of the combustion sequence as stated above, and the creep fatigue damages were evaluated for the last cycle using equation (1).

3. Thermal barrier coating

3.1 Material and processing

Although the effectiveness of the TBC for enhancing the life of a liquid rocket combustion chamber has long been pointed out [1,2], examples of the practical use of the TBC have been very limited, such as Cr/Ni coating of the RD-170 engine [19] and so on. Superior bonding strength of the TBC layer onto the copper alloy substrate is quite necessary to endure huge buckling stress caused by both the extremely high-heat flux from combustion gas and the restriction of the outer shell. Ceramic TBC, such as YSZ (Yttria Stabilized ZrO2), is often used in gas turbines. However, such brittle ceramic TBC cannot be applied to a rocket engine combustion chamber because it buckles and falls off.

In this study, therefore, NiCrAlY which is usually used as a bond coat between a ceramic top coat and a metallic substrate in a gas turbine of a TBC system, was investigated. NiCrAlY coating inside a combustion chamber was formed by atmospheric plasma spraying (APS), and then the coating layer was re-melted by a laser beam and fused to the copper alloy substrate to improve the adhesion strength considerably. Figure 7 shows a cross-sectional photo of NiCrAlY coating layer on a copper alloy substrate before and after the laser re-melting treatment that was observed by SEM (Scanning Electron Microscope). Although some porosities in the coating layer and at the interface between the coating and the substrate were observed before the re-melting process (indicated "as sprayed" in Fig.7), almost no porosities could be seen after the laser re-melting treatment (indicated "re-melted by laser" in Fig.7). The NiCrAlY coating layer was densified, and simultaneously the ingredients of both the coating and the substrate were diffused into each other, resulting in improvement of the bonding strength.

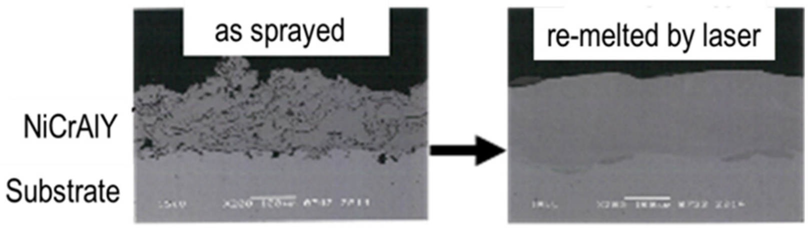

Figure 7: Cross-sectional photo of NiCrAlY coating layer on copper alloy substrate before and after laser re-melting treatment

3.2 Evaluation of thermal conductivity

The thermal conductivity of the laser re-melted NiCrAlY coating layer was evaluated. A NiCrAlY coating layer with a thickness of about 150 μm was formed on a CuCrZr specimen, and the thermal diffusivity was measured by the laser flash method. Thermal diffusivity of the laser re-melted NiCrAlY coating layer (α_{TBC}) on the specimen was determined by Eq. (2) as follows:

$$\alpha_{TBC} = {d_{TBC}}^2 / \tau_{TBC} \tag{2}$$

where

$$\tau_{TBC} = \frac{6(C_{Sb}+C_{TBC})\times A - 6(C_{Sb}+3C_{TBC})\times A_{Sb}}{3C_{Sb}+C_{TBC}} \tag{3}$$

$$C_{Sb} = c_{Sb}\rho_{Sb}d_{Sb} \tag{4}$$

$$C_{TBC} = c_{TBC}\rho_{TBC}d_{TBC} \tag{5}$$

where d_{TBC} is the thickness of the NiCrAlY coating layer, τ_{TBC} is the thermal diffusion time of the NiCrAlY coating layer, c_{Sb} is the specific heat of the substrate, ρ_{Sb} is the density of the substrate, c_{TBC} is specific heat of NiCrAlY, A is the area thermal diffusion time of the whole specimen, and A_{Sb} is the area thermal diffusion time of the substrate. The thermal conductivity of the re-melted NiCrAlY coating layer was then determined by Eq. (6),

$$\kappa_{TBC} = c_{TBC} \times \rho_{TBC} \times \alpha_{TBC} \tag{6}$$

where κ_{TBC}, c_{TBC}, ρ_{TBC}, and α_{TBC} are thermal conductivity, specific heat, density, and thermal diffusivity, respectively.

Because the laser re-melted NiCrAlY coating layer was so thin, it was difficult to measure its specific heat and density. Therefore, specific heat and density of the laser re-melted NiCrAlY coating layer were substituted by using a sprayed thick material of NiCrAlY. Figure 8 shows the thermal conductivity of the re-melted NiCrAlY coating layer on the copper alloy substrate. The thermal conductivity was normalized by that of Cu-A or B at room temperature (see Fig. 3) As can be seen from Fig. 8, a decrease in thermal conductivity around 800 K is observed, but the mechanism of such decrease is unclear at present and detailed analysis should be conducted to determine the thermal conductivity. In this study, life time analysis of a combustion chamber was conducted by using the thermal conductivity data indicated in Fig. 8.

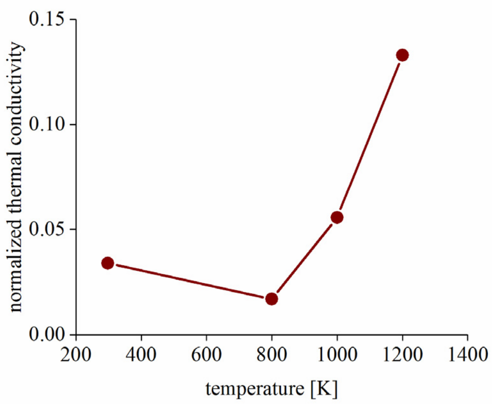

Figure 8 : Thermal conductivity of re-melted NiCrAlY coating layer

3.3 Cyclic combustion gas heating test of TBC

Cyclic heating test of TBC was conducted by using a subscale calorimetric chamber whose inner wall of the throat section was covered with TBC. Figure 9 shows an assembly drawing of the test specimen. The part from contraction section to nozzle section was divided into four parts and the inner surface of the third throat section was covered with TBC. The Inner diameter of the throat was 26 mm. A NiCrAlY TBC layer was formed on the inner surface of the test specimen by APS, and the NiCrAlY layer was re-melted by a laser. Finally, the coating surface was polished and finished by a lapping method to a thickness of 150 μm. Cyclic combustion gas heating test conditions are listed in Table 1.

DOI: 10.13009/EUCASS2017-535

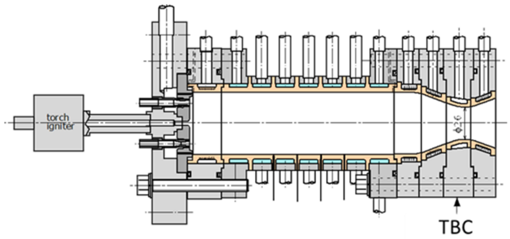

Figure 9 : Assembly drawing of a cyclic combustion gas heating test specimen (TBC was formed on the inner surface of throat section part)

Table 1 : Cyclic combustion gas heating test conditions

Propellant	GOX/GH_2
Coolant	water
Combustion pressure Pc	2 MPa or 2.5 MPa
Mixture ratio	6.5
Steady combustion time	10 sec

The cyclic combustion gas heating tests were terminated after 24 cycles because of the leakage of water from the coolant channel of the contraction section. Figure 10 indicates heat flux and the maximum surface temperature of the TBC calculated from chamber wall temperature measured by thermo-couples. Heat flux was about 21 MW/m^2 and estimated TBC surface temperature was about 1020 K when the chamber pressure Pc was 2 MPa, and heat flux was about 28 MW/m^2 and TBC surface temperature was about 1180 K when Pc was 2.5 Mpa.

Figure 11 shows a photo of a TBC test specimen after cyclic heating tests. As can be seen from Fig.11, there was no damage to the TBC coating layer. Because falling off of the TBC was observed after three cycles of the cyclic combustion gas heating test without a laser re-melting process, the laser re-melting process is very effective. The cyclic combustion gas heating tests will be continued to evaluate the durability of TBC for reusable rocket engine combustion chamber application at the Kakuda Space Center of JAXA.

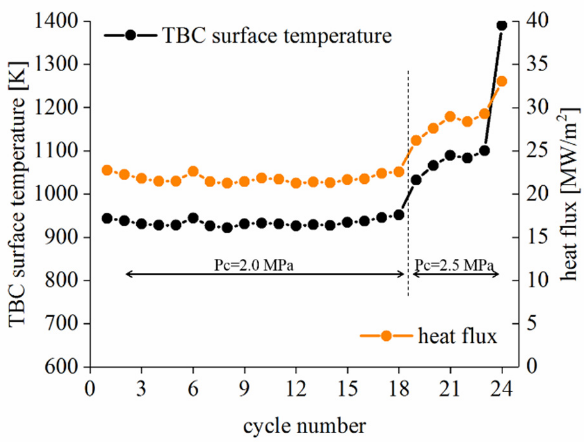

Figure 10 : Heat flux and maximum surface temperature of TBC

DOI: 10.13009/EUCASS2017-535

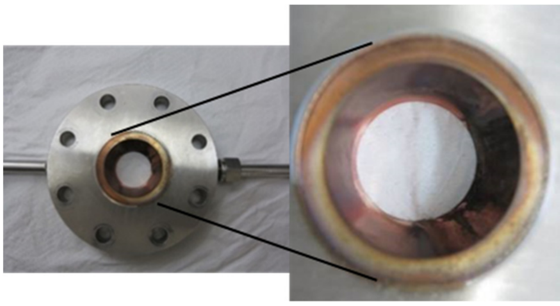

Figure 11 : Appearance of TBC test specimen after cyclic heating test

4. Results

4.1 Effect of material properties of an inner liner

In this section, the effect of material properties of the copper alloy used in the inner liner on creep fatigue damages and lifetime were examined for the models A, B, and C. For all these models, an outer shell made of normal material and no TBC was assumed.

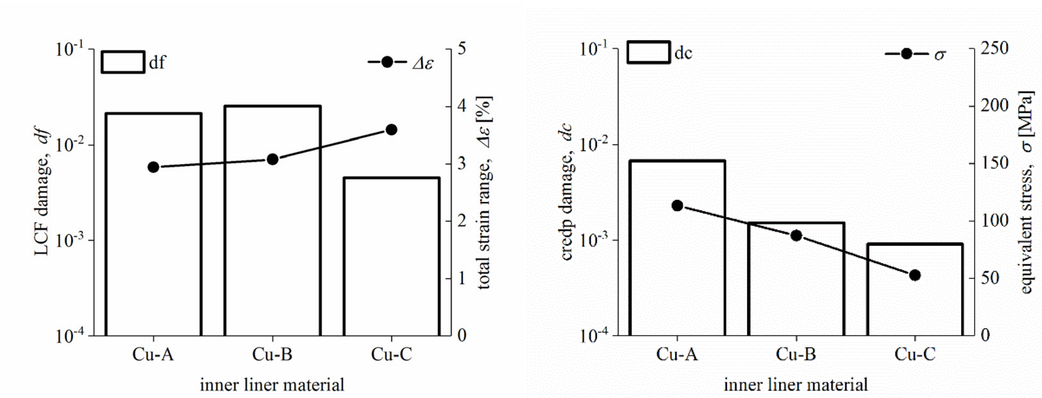

Figure 12: Estimated fatigue damage and strain range (left) and creep damage and average stress (right) for three copper alloys, Cu-A, B, and C of the inner liner

In the graph on the left of Fig. 12, fatigue damage and total total strain range are plotted by a bar graph and a solid line with solid circles, respectively. The strength of the copper alloy reflects the magnitude of the total strain range. The total strain range of Cu-A became smallest because its yield stress is largest, and the total strain range of Cu-C, of which the yield stress is smallest, became largest. However, since the fatigue strength of Cu-C is the largest among the three copper alloys, the fatigue damage was much smaller than those of Cu-A and B.

In the graph on the right of Fig. 12, the creep damage and average equivalent stress during the steady state combustion phase are presented. The average stresses are plotted by a solid line with symbols and become smaller in the order of Cu-A. B, and C. As shown in Fig.4, the yield stresses of these copper alloys decrease in order of Cu-A, B, and C. Hence, for the inner liner with the copper alloy of larger yield stress, the stress level during the steady combustion phase becomes larger. Although the creep strength of Cu-C is smaller than those of Cu-A and B, the effect of low level stress resulted in the smallest creep damage of Cu-C.

In the graph on the left of Fig.13, the total damage estimated at P1 in the inner liner for three copper alloys is plotted with a black line with fatigue (brown line) and creep (blue line) damages. The creep damages were much lower than the fatigue damages, and then the total damage was dominated by fatigue damage for these models. As a result, the lifetime of the chamber wall of model C is longest, around five times longer than the others, as shown in the graph on the right of Fig.13.

DOI: 10.13009/EUCASS2017-535

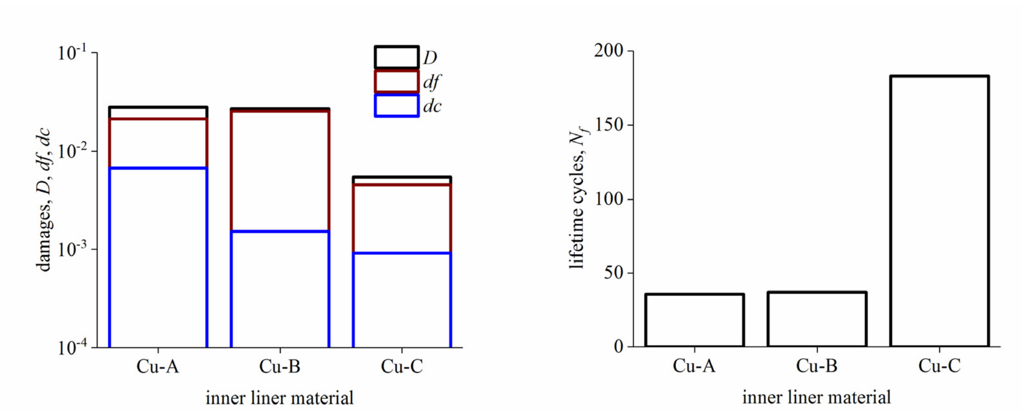

Figure 13: The total, fatigue, and creep damages estimated at P1 of three models (left) and estimated lifetime cycles (right) of the chamber wall for nominal outer shell without TBC

4.2 Effect of a thermal barrier coating

A thermal barrier coating on the surface of the inner liner effectively reduces heat flux from combustion gas and decreases wall temperature. Hence, TBC seems to work generally to improve the lifetime of the chamber wall. However, a decrease of wall temperature caused a rise in the yield stress of the inner liner material and thus increased actual stress level during the steady state combustion phase, resulting in an increase of creep damage. Creep damage and average equivalent stress during a combustion phase are presented in Fig. 14 for the inner liner material Cu-A (left) and Cu-C (right). For both copper alloys, by adding a TBC layer on the inner surface of the chamber wall, the average stress increased. Since the yield stress of Cu-A is much higher than that of Cu-C, the actual stress of Cu-A during steady state combustion showed a much higher increase than that of Cu-C.

On the other hand, the wall temperature decreased remarkably by the addition of a TBC layer on the surface of the inner liner. The decreases of wall temperature from that of the model without TBC were about 90 K for 50 μm and about 140 K for 100 μm, respectively.

Hence, the creep damage of Cu-A for the TBC thickness of 50 μm increased due to the increase of stress level, despite the decrease of wall temperature. For the TBC thickness of 100 μm, the stress almost reached its yield stress and was nearly the same as that of 50 μm. The wall temperature further decreased and thus the creep damage decreased even in model A.

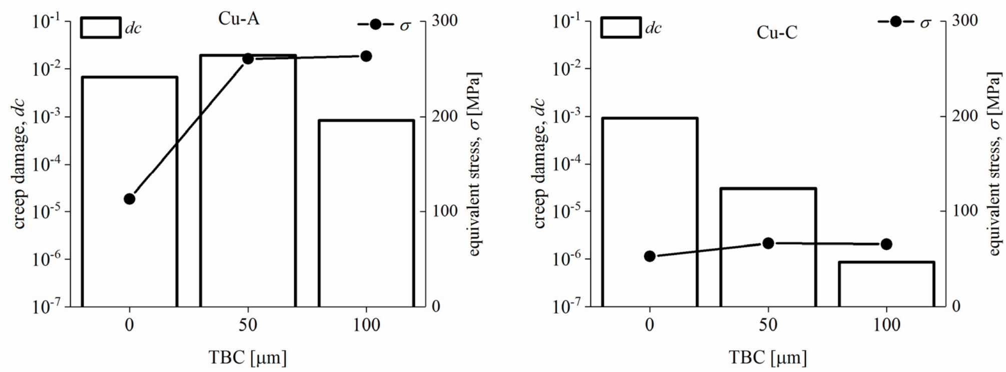

Figure 14; Effect of TBC on creep damage and average stress during the steady state combustion phase for models A and C

Figure 15 presents estimated damages of the total, fatigue, and creep for models A, B, and C. The graph on the left shows damages of the models without TBC, which is the same as in the left of Fig.13. The middle graph and graph on the right show damages for the TBC of 50 μm and 100 μm. Generally, by adding a TBC layer on the surface of the inner liner, total damages decreased. Especially the decrease of creep damage was remarkable, sometimes below that depicted by the graph.

As shown in Fig.14, in model A, the increase of stress due to the decrease of wall temperature resulted in an increase of the creep damage, and the total damage of the model with a 50 μm TBC layer became almost the same as that of the model without a TBC layer.

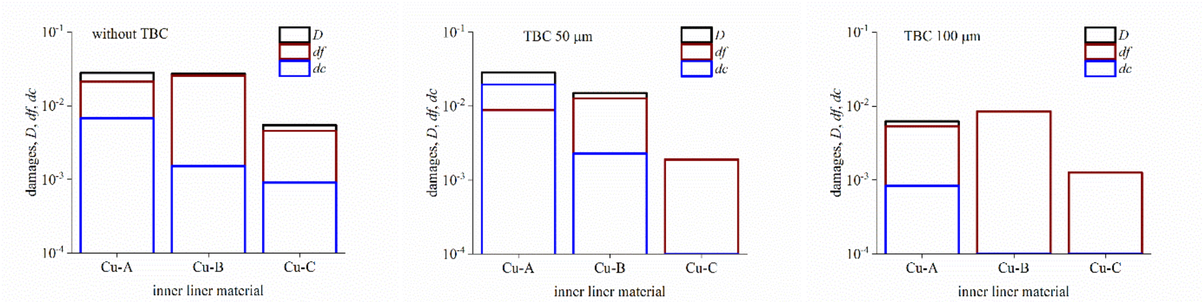

Figure 15: The total, fatigue, and creep damages estimated at P1 of three models. The left graph shows damages without TBC, the middle for 50 μm, and the right for 100 μm

The estimated lifetimes are plotted in Fig. 16 for models A, B, and C with or without TBC. The improved effect of lifetime is clearly seen in models B and C. Especially, the lifetime of the inner liner of model C showed remarkable improvement. Compared with the model without TBC, the lifetime of the model with 100 μm TBC layer was four times of that of the inner liner without TBC.

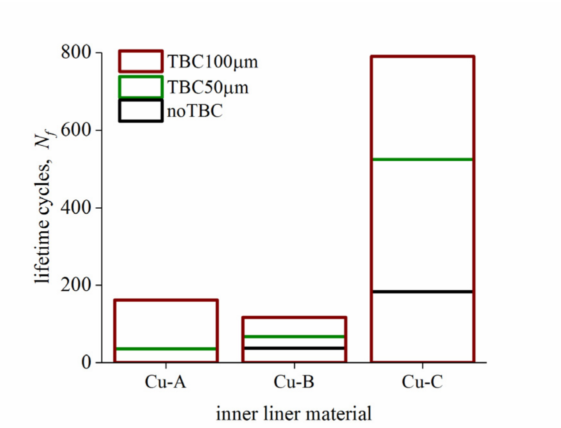

Figure 16: Comparison of lifetimes of the inner liner of three copper alloys with or without TBC

4.3 Effect of a low λ outer shell

Since the inner liner is heated by heat flux from combustion gas and the wall temperature rises, the inner liner tends to expand. On the other hand, the outer shell is cooled by the coolant which flows in coolant channels and tends to contract. In the present chamber wall model in which the outer shell is made of normal material as explained in the section 2.3, the chamber wall showed contraction during the combustion phase. The radial displacement at position P1 of model C in the last combustion cycle is plotted in Fig.17 by a solid black line. In the start-up phase, the chamber wall rapidly contracted and remained an almost constant radius during the steady state combustion phase. The magnitude of contraction during the steady state combustion phase was about -300 μm. After the combustion finished, the chamber started to expand.

In the present simulation, to examine the effect of contraction on damages to the inner liner, a metal material with very low coefficient of thermal expansion was applied to the outer shell. For the model C, Invar was assumed as the material of the outer shell. The calculated radial displacement at position P1 during the last cycle is plotted in Fig. 17 by a brown line. The chamber wall expanded during the start-up phase and showed a behaviour opposite to that of the normal case. The radial displacement during the steady state combustion phase was about +150 μm.

As shown in Fig.17, by using Invar for the outer shell, the magnitude of radial displacement became smaller than that of the model using the normal outer shell, resulting in a decrease of the total strain range in the combustion cycle. In the left graph of Fig.18, the fatigue damage and total strain range are presented for three models. For all models, the total strain ranges were smaller than those of the normal outer shell.

DOI: 10.13009/EUCASS2017-535

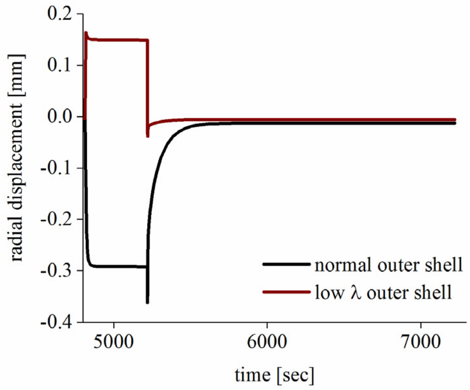

Figure 17: Radial displacement during the 3rd combustion cycle for model C and of the outer shell of normal material and Invar

The low cycle fatigue damage for all models which used Invar as an outer shell material also showed smaller fatigue damages than those of the model of a normal outer shell. In the right graph of Fig.18, the estimated lifetime of the chamber wall for all models are presented. The present simulation results suggested that the lifetime would be extended by using Invar for the outer shell. Especially, the use of Invar for the model in which Cu-C was used as an inner liner material was found to be most effective to extend lifetime.

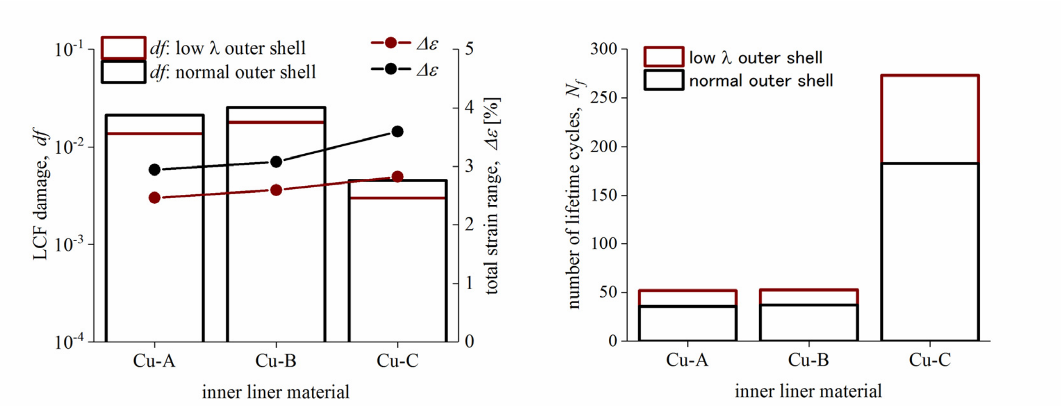

Figure 18: The fatigue damage and total strain range

5. Conclusions

Effects of material properties of the inner liner and outer shell and a thermal barrier coating on the lifetime of a combustion chamber wall of large thrust rocket engines were investigated by calculating creep fatigue damages on the inner liner for repeated firing cycles. Major results of the present work are as follows,

The mechanical properties largely differed according to their manufacturing process and thermal treatment for the same copper alloys with chromium and zirconium. Their differences affected the lifetime cycle of the chamber wall. Especially, the yield stress of the inner liner material is one of the key factors affecting lifetime.

A thermal barrier coating on the surface of the inner liner effectively reduced wall temperature and decreased the fatigue and creep damages, resulting in the extension of the lifetime of the combustion chamber. However, for the copper alloy which has high yield stress, TBC may have the opposite effect of increasing creep damage.

The outer shell of a material with a low coefficient of thermal expansion reduced restriction of the inner liner and may have extended the lifetime of the chamber wall.

The effects due to usage of TBC and a low expansion outer shell on extension of the lifetime will be enhanced by using an inner liner of low yield stress material.

References

[1] Quentmeyer, R. J. 1990. Rocket Combustion Chamber Life-Enhancing Design Concepts. In: 26th *Joint Propulsion Conference and Exhibit*. AIAA 90-2116.
[2] Popp, M. and Schmidt, G. 1996. Rocket Engine Combustion Chamber Design Concepts for Enhanced Life. In: *32nd Joint Propulsion Conference and Exhibit.* AIAA 96-3303.
[3] Sung, I.-K., Northcutt, B.G., Rubel, K.S., and Anderson, W.E. 2003. A Subscale-Based Life Prediction Methodology For Rocket Engine Combustors. In: *39th Joint Propulsion Conference and Exhibit.* AIAA 2003-4900.
[4] Sung, I.-K. and Anderson, W.E., 2005. A Subscale-Based Rocket Combustor Life Prediction Methodology. In: *41st Joint Propulsion Conference and Exhibit.* AIAA 2005-3570.
[5] Riccius, J.R., Bouajila, W., and Zametaev, E., B. 2013. Comparison of Finite Element analysis and experimental results of a combustion chamber type TMF panel test. In: *49th Joint Propulsion Conference.* AIAA 2013-3846.
[6] Riccius, W., Zametaev, E.B., and Bouajila, B. 2014. Inner liner temperature variation caused deformation localization effects in a multichannel model of a generic LRE wall structure. In: *50th Joint Propulsion Conference.* AIAA 2014-3988.
[7] Thiede, R.G., Zametaev, E.B., Riccius, J.R. Fassin, M., and Reese, S. 2015. Comparison of Damage Parameter Based Finite Element Fatigue Analysis Results to Combustion Chamber Type TMF Panel Test Results. In: *51th Joint Propulsion Conference.* AIAA 2015-4070.
[8] Nishimoto, M., Negishi, H., Yoshimura, S., Kasahara, N., Akiba, H., Sunakawa, H., Hori, S., and Negoro, N. 2015. Failure mechanism and life evaluation of liquid rocket engine combustion chamber under sever multi-physics condition. *Transactions of the JSME*, Vol.81, No.826, pp.1-18 (in Japanse).
[9] Amakawa, H., Negishi, N., Nishimoto, M., and Hori, Shunsuke. 2017. Numerical Investigation of Longer Life Combustion Chambers of Liquid Rocket Engines Based on Coupled Thermal-Fluid-Structure Simulation. In: *58th Structures, Structural Dynamics, and Materials Conference.* AIAA 2017-1989.
[10] Kimura, T., Hashimoto, T., Sato, M., Takada, S., Yagishita, T., Naruo, Y., Ogawa, H., Ito, T., Obase, K., Fukuda, Y., and Kai, T. 2015. Firing Tests for the Main Engine of the Reusable Sounding Rocket. In: *Proceedings of 30th International Symposium on Space Technology and Science*.
[11] Kimura, T., Hashimoto, T., Sato, M., Takada, S., Moriya, S., Yagishita, T., Naruo, Y., Ogawa, H., Ito, T., Obase, K., and Ohmura, H. 2016. Reusable Rocket Engine -Firing Tests and Lifetime Analysis of Combustion Chamber. *Journal of Propulsion and Power.* 32: 1087-1094.
[12] Ito, T., Nonaka, S., and Ogawa, H. 2015. Progress of Technical Demonstrations for Reusable Sounding Rocket System. In: *Proceedings of 30th International Symposium on Space Technology and Science*.
[13] Kurosu, A., Yamanishi, N., Sunakawa, H., Nishimoto, M., and Okita, K. 2008. LE-X -Japanese Next Liquid Booster Engine. In: 44th *Joint Propulsion Conference and Exhibition.* AIAA 2008-4665.
[14] Sunakawa, H., Nishimoto, M., Yamanishi, N., Noda, Keiichiro, Sato, E., and Shiwa, M. 2011. Reliability and Life Time Evaluation Approach of the LE-X Engine. In: 47th *Joint Propulsion Conference and Exhibition.* AIAA 2011-5933.
[15] Gordon, S. and McBride, B. J. 1976. Computer Program for Calculation of Complex Chemical Equilibrium Compositions, Rocket Performance, Incident and Reflected Shocks, and Chapman-Jouguet Detonations. *NASA SP-273*.
[16] Bartz, D.R. 1957. A Simple Equation for Rapid Estimation of Rocket Nozzle Convective Heat Transfer Coefficients. *Jet Propulsion*, Jan. 49-51.
[17] Ellis, D. and Michal, M. 1996. Mechanical and Thernal Properties of Two Cu-Cr-Nb Alloys and NARloy-Z. NASA CR-198529.
[18] Ellis, D, 2005, GRCop-84 : A High-Temperature Copper Alloy for High-Heat Flux Applications. NASA TM-2005-213566.
[19] Fedorov, V., Chvanov, V., Chelkis, F., Polyansky, A., Ivanov, N., Lozino-Lozinskaya, I., and Buryak, A. 2006. The Chamber Cooling System of RD-170 Engine Family: Design, Parameters, and Hardware Investigation Data, In: *42nd Joint Propulsion Conference and Exhibit.* AIAA 2006-4363.